J Neurophysiol 113: 2164–2172, 2015.
First published January 14, 2015; doi:10.1152/jn.00569.2014.

Comparative diffusion tractography of corticostriatal motor pathways reveals differences between humans and macaques

S. F. W. Neggers,[1] B. B. Zandbelt,[2,3] M. S. Schall,[2] and J. D. Schall[2]

[1]*Brain Center Rudolf Magnus, Department of Psychiatry, University Medical Centre, Utrecht, The Netherlands;* [2]*Department of Psychology, Vanderbilt Vision Research Center, Center for Integrative and Cognitive Neuroscience, Vanderbilt University, Nashville, Tennessee; and* [3]*Donders Institute for Brain, Cognition and Behaviour, Radboud University, Nijmegen, The Netherlands*

Submitted 1 August 2014; accepted in final form 8 January 2015

Neggers SF, Zandbelt BB, Schall MS, Schall JD. Comparative diffusion tractography of corticostriatal motor pathways reveals differences between humans and macaques. *J Neurophysiol* 113: 2164–2172, 2015. First published January 14, 2015; doi:10.1152/jn.00569.2014.—The primate corticobasal ganglia circuits are understood to be segregated into parallel anatomically and functionally distinct loops. Anatomical and physiological studies in macaque monkeys are summarized as showing that an oculomotor loop begins with projections from the frontal eye fields (FEF) to the caudate nucleus, and a motor loop begins with projections from the primary motor cortex (M1) to the putamen. However, recent functional and structural neuroimaging studies of the human corticostriatal system report evidence inconsistent with this organization. To obtain conclusive evidence, we directly compared the pattern of connectivity between cortical motor areas and the striatum in humans and macaques in vivo using probabilistic diffusion tractography. In macaques we found that FEF is connected with the head of the caudate and anterior putamen, and M1 is connected with more posterior sections of the caudate and putamen, corroborating neuroanatomical tract tracing findings. However, in humans FEF and M1 are connected to largely overlapping portions of posterior putamen and only a small portion of the caudate. These results demonstrate that the corticobasal connectivity for the oculomotor and primary motor loop is not entirely segregated for primates at a macroscopic level and that the description of the anatomical connectivity of corticostriatal motor systems in humans does not parallel that of macaques, perhaps because of an expansion of prefrontal projections to striatum in humans.

comparative anatomy; DTI; human; macaque; oculomotor

THE GOAL OF THIS STUDY WAS to compare connectivity between cortical motor areas and the striatum in human and macaque. The classic description of basal ganglia organization is derived from anatomical and physiological findings in macaques that have emphasized segregated loops subserving motor, oculomotor, cognitive, and limbic control with the motor loop passing through the putamen and the oculomotor loop through the caudate nucleus (Alexander et al. 1986).

Although derived primarily from nonhuman primate studies, this organization is applied to the human brain in textbooks (e.g., Purves et al. 2011; Kandel et al. 2012) and models of neuropsychiatric diseases (e.g., Rodriguez-Oroz et al. 2009; Kennard and Nachev 2005). Such extrapolation should be balanced by the obvious differences between macaque and human brains. The human brain is not only much larger but also has a disproportionately larger frontal cortex (Fuster 2008; Passingham and Wise 2012), reflected in a higher degree of cortical folding and a greater increase thereof along the brain's anterior-posterior (A-P) axis (Zilles et al. 1988, 1989). The expansion of frontal cortex in primate evolution may have influenced corticostriatal connectivity along the A-P axis.

Furthermore, results from several recent human neuroimaging studies are inconsistent with a strict segregation of effector systems between the caudate and putamen. For example, high-resolution functional (f)MRI studies have demonstrated more activation in the putamen than the caudate during simple saccadic eye movements (Dejardin et al. 1998; Krebs et al. 2010; Neggers et al. 2012). Also, diffusion tensor imaging (DTI) tractography showed that human frontal eye fields (FEF) are connected to putamen more than to the caudate (Neggers et al. 2012). The strict subdivision of the caudate and putamen into oculomotor and skeletomotor loops is an oversimplification even for macaques. Histological tracing studies from the FEF and supplementary eye field (SEF) have found terminal labeling in the caudate and putamen (Parthasarathy et al. 1992; Calzavara et al. 2007), and single-unit activity in putamen is associated with saccadic eye movements (Phillips and Everling 2012).

The obvious differences between macaque and human brains and the variation of results across studies call for a direct comparison of corticostriatal connectivity between humans and macaques using the same technique. Here, we studied fiber pathways from FEF and M1 to ipsilateral caudate and putamen in macaques and humans using probabilistic diffusion tractography, a technique that has been validated against histological tracing (Dyrby et al. 2007).

We hypothesize that oculomotor and skeletomotor corticostriatal pathways do not exclusively connect with the caudate and putamen, respectively, but run through both structures with denser termination in putamen in humans. We further hypothesize that the greater volume and A-P gyrification of prefrontal cortex in humans is paralleled by oculomotor and skeletomotor corticostriatal pathways projecting to more posterior striatal regions in humans vs. macaques. If true, then these differences should be largest for corticostriatal connections originating in posterior frontal cortex (e.g., FEF and M1) but smaller, if any, for connections originating in regions in anterior frontal cortex, such as the frontal pole. We therefore also reconstructed fibers between frontal pole and the caudate and putamen.

Address for reprint requests and other correspondence: S. F. Neggers, Brain Center Rudolf Magnus, Dept. of Psychiatry, Univ. Medical Centre (UMC), Utrecht, Utrecht, The Netherlands (e-mail: b.neggers@umcutrecht.nl).

METHODS

Participants

Nine adult *Macaca radiata* (age 6–8 yr, 7 males) were scanned at Vanderbilt University Institute of Imaging Science. Animal care exceeded policies set forth by the US Department of Agriculture and Public Health Service Policy on Humane Care and Use of Laboratory Animals. All procedures were conducted with supervision and approval from the Vanderbilt Institutional Animal Care and Use Committee.

Nine healthy humans (age 20–35 yr, 5 men) were scanned at the University Medical Centre (UMC) Utrecht. Written informed consent was obtained and procedures were approved by the UMC Utrecht Ethics Committee.

Data Acquisition

The same model of Philips Achieva 3T MRI scanners and similar pulse sequences were used at Vanderbilt and UMC Utrecht. Spatial and temporal details and coil layout were adapted to head size.

Humans. Data of nine subjects were randomly picked from the complete dataset of a previous study (Neggers et al. 2012). Two single shot echo planar imaging (EPI)-DTI scans were acquired covering the whole brain, consisting of 30 diffusion-weighted scans (b = 1,000 s/mm^2) with noncolinear gradient directions and one average (B0-image) of five diffusion unweighted scans (b = 0 s/mm^2); repetition time (TR), 7,035; echo time (TE), 68 ms; matrix, 128 × 128; 1.875 × 1.875 mm^2 in-plane resolution; 75 axial slices, phase encoding direction, PA (A-P 2nd scan); slice thickness, 2 mm, no slice gap; field of view (FOV), 240 × 240 × 150 mm^3; SENSE factor 3; EPI factor, 35; and no cardiac gating. DTI was measured twice with phase encoding direction reversed the second time to correct for susceptibility-induced spatial distortions known to occur in such images (Andersson and Skare 2002). A high-resolution T1-weighted structural scan covering the whole brain was acquired: TR, 9.87 ms; TE, 4.6 ms; flip angle, 8°; FOV, 224 × 224 × 160 mm^3; matrix, 256 × 256; in-plane resolution, 0.875 × 0.875 mm^2; 200 axial slices; and slice thickness 1 mm, no slice gap. This scan was used to register with the DTI data and normalize the data to template space (see *Image preprocessing*).

Macaques. Seven of the macaques were scanned in sphinx position with their head placed in a plastic stereotactic frame. Two of the macaques were scanned in supine position without the frame. Four circular FLEX receive coils were arranged pairwise along an A-P and left-right axis. Macaques were sedated (induction) with 10 mg/kg of ketamine and maintained during acquisition with a 1–2% isoflurane: oxygen mixture. Scans consisted of four (5 for 1 macaque) consecutive single shot EPI-DTI with 32 diffusion-weighted scans (b = 1,000 s/mm^2) for each subsequent scan with noncolinear gradient directions and one diffusion unweighted scan (B0-image, b, 0 s/mm^2; TR, 6,800 ms; TE, 75 ms; matrix, 128 × 128; in-plane resolution, 1.5 × 1.5 mm^2; 40 axial slices; phase encoding direction, A-P; slice thickness, 1.5 mm, no gap; FOV, 192 × 192 × 60 mm^3; SENSE factor 2; EPI factor, 67; no cardiac gating). A high-resolution whole brain T1-weighted structural scan was also acquired (TR, 9.87 ms, TE, 4.6 ms; flip angle, 8°; FOV, 224 × 224 × 160 mm^3; matrix, 256 × 256; in-plane resolution, 0.875 × 0.875 mm^2; 200 axial slices; and slice thickness, 1 mm, no gap).

Data Analysis

Image preprocessing. DTI images were preprocessed with an automated six-step procedure, using registration algorithms from SPM8 (www.fil.ion.ucl.ac.uk/spm/). First, the two human DTI scans were merged and corrected for susceptibility-induced image distortions using an in-house toolbox (see Neggers et al. 2012). Because there was hardly any image distortion in the macaque DTI scans, multisession averaging was performed during probabilistic fiber tracking (see below) as to maximize the signal-to-noise ratio. Second, from the B0 images we created a preliminary brain mask. A custom procedure was used that included voxels with an intensity higher than half the average volume intensity, to remove nonbrain tissue (muscle, skin) from the T1-weighted and DTI images. The mask was dilated three times using the default kernel in SPM8 that dilates one voxel each in the x, y, and z dimensions. Third, the masked T1-weighted image was coregistered to the B0 image using mutual information coregistration. Fourth, the masked coregistered T1-weighted image was segmented into gray matter, white matter, and cerebrospinal fluid using the "unified segmentation" algorithm (Ashburner et al. 2005) in combination with species-specific population-based probabilistic tissue type maps (Rex et al. 2003; McLaren et al. 2009). It has been demonstrated that this approach for segmentation, originally designed for human MRI image segmentation, is efficient for macaques as well, provided the correct macaque prior information atlases are used for each tissue type (McLaren et al. 2010). This procedure also estimates parameters for warping reconstructed fiber images from diffusion-weighted native space to species template space and vice versa. Fifth, with the use of these parameters the T1-weighted image was normalized to the International Consortium for Brain Mapping template for humans and to the template from McLaren et al. (2009) for macaques (referred to as the 112RM-SL space) and finally resliced (macaques: 0.7 × 0.7 × 0.7 mm^3; humans: 1 × 1 × 1 mm^3). This normalized image was also used for defining fiber tracking seeds and creating caudate and putamen segmentations. Raw DTI scans were not normalized, as DTI tensor fitting must be performed in native space, but rather fiber tracking results were normalized. Sixth, we created a more precise and final brain mask by combining segmented gray and white matter images. It was used to mask native T1-weighted and DTI images to prevent spurious out-of-brain deviations during fiber tracking.

Cortical seeds and waypoint masks. To identify oculomotor and skeletomotor corticostriatal pathways, we determined the location of FEF and M1 in both species. For topographic comparison, we defined a seed region in the frontal pole. Seed regions were defined as spheres with a 2-mm (macaques) or 4-mm (humans, only frontal pole seed needed to be larger to obtain any connections) radius centered on the gray-white matter boundary in the anatomical scan normalized to Montreal Neurological Institute (MNI) space (112RM-SL space for macaques) and then warped to native space using inverse normalization. Figure 1*A* shows the cortical seeds.

HUMAN. The FEF seed ($x = \pm 28$, $y = -5$, $z = 54$) was identified as the local maximum of a group fMRI activation map involving simple saccades (Neggers et al. 2012). It is located just ventral of the junction of the precentral sulcus and superior frontal sulcus, a region now accepted as human homologue of macaque FEF (Amiez et al. 2006; Neggers et al. 2012). The M1 seed ($x = \pm 33$, $y = -21$, $z = 58$) was identified as the local maximum of a group fMRI activation map distinguishing oculomotor and skeletomotor systems (Connolly et al. 2007), located in the precentral gyrus in a knob-like structure identified as the area containing motor thumb functions (Yousry et al. 1997). The frontal pole seed was defined as the gray-white matter boundary of the most anterior part of the cortex coinciding with a horizontal plane skimming the superior caudate nucleus surface ($x = \pm 15$, $y = 54$, $z = 22$).

MACAQUE. The FEF seed ($x = \pm 13$, $y = 28$, $z = 26$) was identified at the dorsal fundus of the anterior bank of the arcuate sulcus, and the M1 seed ($x = \pm 17$, $y = 17$, $z = 28$) was identified as the thumb area (Saleem and Logothetis 2012; Paxinos 1999). The frontal pole seed ($x = \pm 6$, $y = 43$, $z = 23$) was defined as described above for humans.

For each seed region, we determined a waypoint mask (Behrens et al. 2007) that fiber tracts had to pass through to be accepted (Fig. 1*B*). Waypoint masks were defined as orthogonal planes in MNI space for humans (FEF and M1: $z = 35$; frontal pole, $y = 37$;) or 112RM-SL space for macaques (FEF and M1: $z = 23$; frontal pole, $y = 34$).

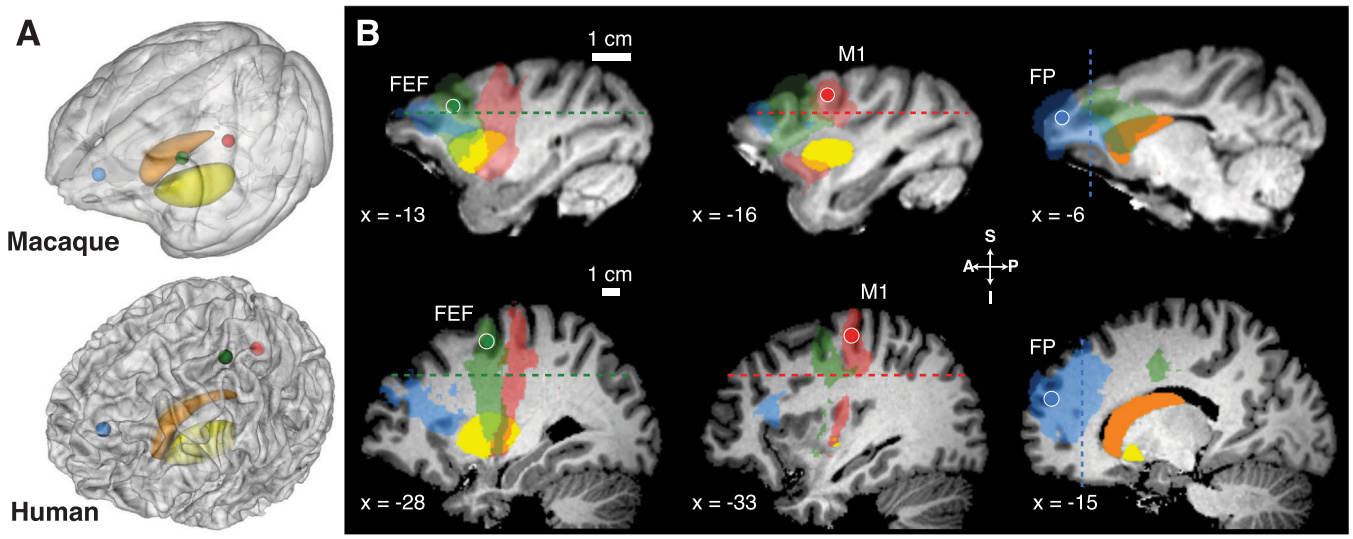

Fig. 1. Cortical seeds, striatal targets, waypoint masks, and corticostriatal streamlines in macaques and humans. Seed regions were defined as spheres with a 2-mm (macaques) or 4-mm (humans) radius. *A*: semitransparent 3-dimensional rendering from the T1-weighted image for macaques (*top*) and humans (*bottom*) with embedded caudate (orange) and putamen (yellow) and cortical seed regions: frontal eye fields (FEF) (green), M1 (red), and frontal pole (FP; blue). *B*: sagittal slices for macaques (*top*) and humans (*bottom*) with overlaid cortical seed regions (FEF, *left columns*), M1 (*middle columns*), and frontal pole (*right columns*), the group-averaged fiber streamlines from these regions (transparent corresponding colors), and the striatal regions caudate (orange) and putamen (yellow). Dashed lines show waypoint mask planes. Slice coordinates are in template space [Montreal Neurological Institute (MNI) space for humans, 112RM-SL space for macaques]. A, anterior; I, inferior; P, posterior; S, superior.

The horizontal waypoint masks separate the cortical sheet containing the FEF and M1 seeds from the striatum. These waypoint masks exclude tracts going from the cortical seeds to other cortical areas, restricting the search to fibers traveling from FEF/M1 to the striatum or other areas below the plane. The vertical waypoint mask plane does the same for streamlines consituting FP-striatal connectivity.

Caudate and putamen segmentation. For seed-based classification analysis (Behrens et al. 2003), we created masks of the left and right caudate and putamen through manual segmentation in all individual normalized T1-weighted images (Fig. 1*A*, orange and yellow surfaces), using MRIcron (http://www.mccauslandcenter.sc.edu/mricro/mricron).

Probabilistic fiber tracking. Probabilistic fiber tracking analysis was performed using FMRIB's Diffusion Toolbox (Behrens et al. 2003, 2007; Smith et al. 2004) running in FSL v4.1.7 (http://fsl.fmrib.ox.ac.uk). This method allows modeling of crossing fibers. In probabilistic fiber tracking, maps of the probability for each voxel of being connected to a prespecified seed region are computed by following the several main diffusion directions in a step by step fashion over voxels, using a so called "ball and stick" model of isotropic and anisotropic diffusion patterns. In seed-based classification analysis (Behrens 2003, 2007) as performed in our study, probability maps are created within a prespecified mask (here the caudate and putamen). The value of a certain voxel in this map reflects the number of streamlines (out of 5,000) that reach that voxel from a certain seed location.

First, the diffusion model was fitted to diffusion-weighted data in native space. For macaques, the model was fitted to DTI data from all four or five sessions at once to average out noise.

Subsequently, 12 (4 striatal regions $\times$ 3 cortical regions) probability maps were created for the left and right caudate and putamen paired with three cortical seed locations per hemisphere (FEF, M1, and frontal pole) by applying seed-based classification fiber tracking, limited to streamlines passing through the waypoint masks. The main parameters for FSL fiber tracking were minimum curvature threshold = 80°, number of steps per sample = 2,000, step length = 0.5 mm, and number of streamlines released = 5,000.

Twelve individual native space classification maps and reconstructed fiber tracts were normalized and resliced to template space (MNI space for humans, 112RM-SL space for macaques). Group-based probability maps were created by counting, for each voxel, the number of participants where this voxel's connection probability was suprathreshold (on the single subject level) divided by the number of participants. A value of 0 implies no connections for any subject, and 1, a connection for all subjects. On the single subject level, a binarization threshold of 7 arriving streamlines (out of 5,000 released from each voxel in the cortical seed region) had to be reached for each monkey for each voxel to be counted as connected. This low value results in tagging a voxel as connected even for a small number of arriving streamlines, yielding connectivity results similar to tracer studies (Parthasarathy et al. 1992; Calzavara et al. 2007). The values in a single subject probability map, which are the numbers of streamlines arriving per voxel, depend on the distance from the seed (counted in voxels), which is greater for humans despite the fact that we could use smaller absolute voxel size in macaque data acquisition. To counter this bias against tracking distance, we adjusted the threshold of minimum streamline count for tagging a voxel as connected for humans such that an equal number of streamlines can reach the mask. To do so, we estimated the relative portion that a 1-cm^2 surface occupies on a sphere with a radius equal to the distance from FEF to the dorsal surface of the striatum in each species (measured in voxels). The ratio of this surface area for both species (16 macaque per 1 human streamline arriving at the 1-cm^2 surface) should reflect the ratio of streamline densities arriving in a unit surface area for fiber tracking in an isotropically diffusive medium. In other words, the ratio reflects how much less likely it is for the larger human brain to receive streamlines in the striatum from the FEF seed, per surface unit. The human binarization threshold was obtained by dividing 7, the monkey binarization threshold, with this ratio, which yielded the (rounded up) value of 0.5 for the human binarization threshold. We believe this procedure corrects adequately for the distance bias that is unavoidable when comparing species with such different brain sizes.

We used a low threshold so as not to remove any potentially interesting findings (for a rationale, see Markov et al. 2013). Importantly, at present no formal method exists for thresholding single subject streamline counts and subsequent group analysis in probabilistic fiber tracking. To demonstrate robustness against (low) threshold choice, we repeated the entire analysis with the twofold and threefold streamline thresholds at the single subject level and various probabil-

ity thresholds at the group level. Also, we systematically varied the minimum curvature angle to establish whether our results are robust against allowed "sharpness" of bends during fiber tracking.

Descriptive and Inferential Statistics

To compare corticostriatal connectivity between macaques and humans, we computed three descriptive statistics based on data pooled across hemispheres.

First, to compare corticostriatal connectivity between the caudate and putamen in thresholded single subject probability images, we computed a connectivity index (I_C):

$$I_C = (V_{caudate} - V_{putamen}) / (V_{caudate} + V_{putamen})$$

where $V_{caudate}$ and $V_{putamen}$ are the proportion of voxels in the caudate and putamen that were connected with a cortical region of interest (ROI). Values closer to 1 indicate stronger connectivity with the caudate than putamen; values closer to −1 indicate stronger connectivity with putamen. Statistical analysis of connectivity indices involved Mann-Whitney *U* -tests (Bonferroni-corrected for multiple comparisons across cortical ROIs).

Second, to compare the distribution of connectivity along the A-P axis, we computed the probability density of corticostriatal connectivity separately for the caudate and the putamen. In each coronal slice, we computed the number of voxels that were connected with a cortical ROI as a fraction of the total caudate or putamen volume. Because the number of coronal slices differed between species, we normalized the A-P distance across species by expressing the coronal slice number as a percentile (anterior-most = 0%; posterior-most = 100%). The A-P slice percentile with maximum connectivity ($P_{A\text{-}P,max}$) was defined as the mode of this probability density function. Statistical analysis of $P_{A\text{-}P,max}$ involved Mann-Whitney *U*-tests (Bonferroni-corrected for multiple comparisons across cortical and striatal ROIs).

Third, to analyze the degree of overlap of projections from FEF and M1 in the striatum in thresholded single subject maps of the left and right caudate and putamen, we computed an overlap index (I_O):

$$I_O = 2\frac{|P_{FEF} \cap P_{MI}|}{|P_{FEF}| + |P_{MI}|}$$

where P_{FEF} denotes the set of voxels connected to the FEF and P_{M1} the set of voxels connected to M1. The numerator is the size of the union of both patches, and the denominator is the sum. Overlap index values near 0 indicate no overlap of FEF and M1 connections. Values closer to 1 indicate greater overlap. Distributions of I_O were compared through two-tailed one-sample *t*-tests corrected for multiple comparisons.

RESULTS

Figure 1 shows the cortical seeds, striatal targets, and group-averaged streamlines between them that pass through the waypoint masks. The general A-P topography of corticostriatal connectivity is evident. Figure 2 shows a map of termination zones of corticostriatal pathways from FEF, M1, and the frontal pole for macaques and humans, overlayed on an axial slice through the striatum of an average normalized T1-weighted MRI scan. Some overlap in termination zones can be discerned superimposed on the A-P topography. Figure 3 shows the patterns of corticostriatal connectivity along the A-P axis. Table 1 reports descriptive and inferential statistics of the comparison between humans and macaques for the connectivity index (I_C) and points along the A-P axis with maximum connectivity ($P_{A\text{-}P,max}$).

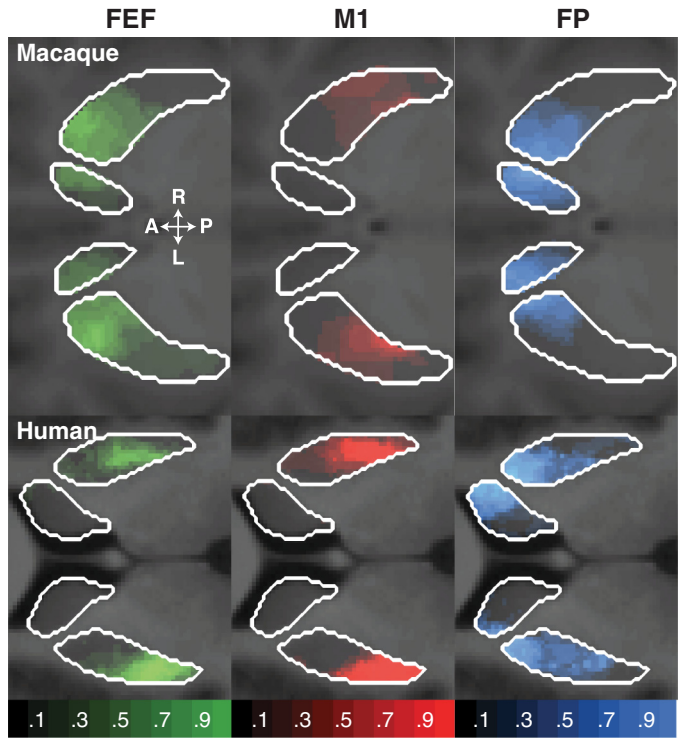

Fig. 2. Classification maps of the probability a cortical seed was connected to the putamen and caudate nucleus, overlaid on 2-dimensional slices through the average normalized T1-weighted scan at the level of the striatum. The opacity of the overlay indicates the probability of connectivity (transparent voxels have a probability equal to 0; opaque voxels have a probability equal to 1).

Oculomotor and Skeletomotor Corticostriatal Pathways

Oculomotor corticostriatal pathways differed between macaques and humans both in the distribution of connections with the caudate and putamen and in the distribution of connections along the A-P axis (*left columns* of Table 1 and Figs. 2–3). The FEF in macaques connects to the caudate and putamen to a similar degree, whereas the FEF in humans more densely connects with putamen than with the caudate. Moreover, the FEF in macaques connects with anterior striatal regions, such as the caudate head and anterior putamen, whereas the FEF in humans connects with much more posterior striatal regions, such as a small part of the caudate body and posterior putamen.

Motor corticostriatal pathways originating from M1 differed between macaques and humans both in the distribution of connections with the caudate and putamen and in the distribution of connections along the caudate A-P axis (*middle columns* of Table 1 and Figs. 2–3). M1 in macaques connects to the caudate and putamen to a similar degree, whereas M1 in humans more densely connects with the putamen than caudate. Furthermore, in macaques fibers from M1 terminated uniformly along the caudate head and the caudate body and central portions of the putamen, whereas in humans these fibers terminate in more posteriorly in the caudate body and in comparable portions of the putamen.

Thus, compared with macaques, human oculomotor and skeletomotor corticostriatal fibers terminate more densely in the putamen than caudate and terminate in much more poste-

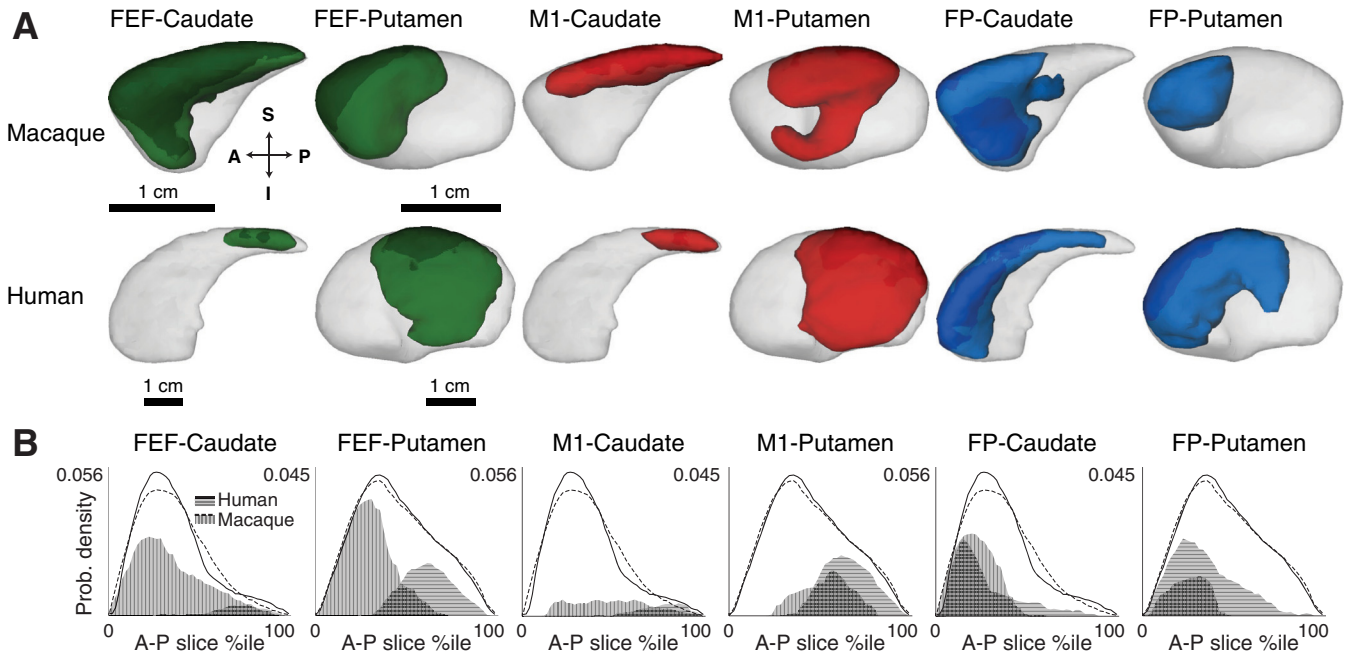

Fig. 3. Classification analysis of corticostriatal fibers in macaque and human. *A*: corticostriatal terminations in macaque (*top*) and human (*bottom*), pooled across hemispheres displayed on left-right (L-R) side views of caudate and putamen. Opaque colors indicate fiber termination zones based on group probability maps thresholded at $P > 0.2$. Arrows show orientation. *B*: distribution of corticostriatal connectivity and striatal volumes along the anterior-posterior (A-P) axis. Line charts show probability densities of total striatal volume along the A-P axis for macaque (dashed lines) and human (solid lines). The total area under the line charts represents the total striatal volume. Area charts show probability densities of corticostriatal connectivity along the A-P axis for macaque (vertically striped areas) and human (horizontally striped areas). For comparison across species and striatal regions, volume and fiber termination densities were normalized, so that the area under the line charts is equal to 1.

rior regions of the striatum, especially for connections from the FEF.

Anterior Prefrontal-Striatal Pathways

If the difference in corticostriatal oculomotor and skeletomotor pathways is a result from the expansion that frontal cortex has undergone in primate evolution, then these differences should be largest for corticostriatal connections originating in posterior frontal cortex (e.g., FEF and M1) but much smaller, if any, for connections originating from the anteriormost regions of frontal cortex. To test this, we analyzed corticostriatal connections originating in the frontal pole. Although there were differences between macaques and humans in their termination density in the caudate vs. putamen, we did not find differences in the distribution along the A-P axis (*right columns* of Table 1 and Figs. 2–3). Frontal pole in macaques terminated more in the caudate than putamen, whereas frontal pole in humans showed similar connectivity with the caudate and putamen. Importantly, however, the distribution of connections along the A-P axis was similar across macaques and humans.

Overlap of Oculomotor with Skeletalmotor Corticostriatal Termination Zones

To test the degree of segregation of the terminations from FEF and M1 to striatum, we quantified the amount of overlap between M1 and FEF connection zones in the striatum with respect to the sum of the areas of the striatum that were connected to either M1 or FEF (index I_O). We observed larger overlap of FEF and M1 corticostriatal terminations in humans compared with monkeys for the putamen [$I_{O,macaque} = 0.18$, $I_{O,human} = 0.52$, $T(8) = 5.23$, $P < 0.0005$] but not caudate [$I_{O,macaque} = 0.24$, $I_{O,human} = 0.55$, $T(8) = 1.42$, $P = 0.096$]. This indicates that skeletomotor and oculomotor corticostriatal pathways are not segregated but overlapping, especially for humans.

Robustness of Findings

In additional analyses, we tested the robustness and generality of these findings. Specifically, we determined to what extent corticostriatal connectivity depends on the three types of thresholds we used: the streamline threshold (minimum number of corticostriatal for tagging a voxel as connected), a

Table 1. *Connectivity indexes and maximum anterior-posterior termination zone of corticostriatal fibers in macaques and humans*

	FEF					M1					FP				
	Macaque	Human	*U*	*P*	Tail	Macaque	Human	*U*	*P*	Tail	Macaque	Human	*U*	*P*	Tail
I_C	0.33 (0.61)	−0.69 (0.17)	81	2.1×10^{-5}*	r	−0.22 (0.60)	−0.69 (0.13)	72	2.0×10^{-3}*	r	0.62 (0.56)	−0.11 (0.27)	78	2.9×10^{-4}*	b
Caudate $P_{A\text{-}P,max}$	27 (13)	74 (21)	12	5.3×10^{-3}*	l	58 (21)	78 (13)	13	7.1×10^{-3}*	l	20 (18)	12 (5)	61	7.7×10^{-2}*	b
Putamen $P_{A\text{-}P,max}$	24 (15)	62 (5)	0	2.1×10^{-5}*	l	55 (23)	63 (5)	23	6.5×10^{-2}	l	30 (30)	24 (5)	54	2.5×10^{-1}	b

I_C, connectivity index; $A\text{-}P_{max}$, maximum anterior-posterior termination zone. Numbers in Macaque and Human columns represent medians with interquartile ranges in parentheses. *U* indicates the Mann-Whitney *U*-test statistic, and *P* gives the *P* value. Tail indicates whether a left-tailed (l), right-tailed (r), or two-tailed (b) test was used (see hypotheses). This analysis was done with streamline binarization thresholds 7 (macacques) and 0.5 (humans). *Statistically significant *P* values, Bonferroni-corrected for multiple comparisons.

Table 2. *Connectivity indices and maximum anterior-posterior termination zone of corticostriatal fibers in macaques and humans for higher streamline thresholds*

	FEF					M1					FP				
	Macaque	Human	*U*	*P*	Tail	Macaque	Human	*U*	*P*	Tail	Macaque	Human	*U*	*P*	Tail
Binarization threshold: 14 (macacques), 1 (human) #fibers															
I_C	0.55 (0.91)	−0.70 (0.22)	77	2.5×10^{-4}*	r	−0.19 (0.75)	−0.70 (0.16)	67	9.4×10^{-3}*	r	0.76 (0.54)	−0.14 (0.30)	78	2.9×10^{-4}*	b
Caudate $P_{A\text{-}P,max}$	23 (18)	75 (17)	4	2.5×10^{-4}*	l	59 (6)	81 (9)	9	1.9×10^{-3}*	l	15 (14)	12 (4)	47	6.1×10^{-1}	b
Putamen $P_{A\text{-}P,max}$	21 (12)	64 (3)	0	2.1×10^{-5}*	l	61 (14)	64 (6)	29	1.6×10^{-1}	l	28 (32)	21 (7)	53	2.9×10^{-1}	b
Binarization threshold: 21 (macaques), 1.5 (human) #fibers															
I_C	0.69 (1.10)	−0.69 (0.22)	76	3.9×10^{-4}*	r	−0.24 (0.89)	−0.72 (0.17)	58	7.8×10^{-4}*	r	0.62 (0.56)	−0.15 (0.33)	44	7.0×10^{-3}*	b
Caudate $P_{A\text{-}P,max}$	26 (19)	75 (16)	4	2.5×10^{-4}*	l	57 (10)	77 (14)	11	3.9×10^{-3}*	l	16 (31)	10 (6)	59	1.1×10^{-1}	b
Putamen $P_{A\text{-}P,max}$	21 (12)	64 (5)	0	2.1×10^{-5}*	l	61 (26)	64 (7)	34	2.9×10^{-1}	l	34 (71)	23 (5)	73	2.5×10^{-3}*	b

Values represent the same analysis outcome as in Table 1, apart from the binarization thresholds that were increased with a factor of 2 and 3. Numbers in Macaque and Human columns represent medians with interquartile ranges in parentheses. *U* indicates the Mann-Whitney U-test statistic, and *P* gives the *P* value. Tail indicates whether a left-tailed (l), right-tailed (r), or two-tailed (b) test was used (see hypotheses). *Statistically significant *P* values, Bonferroni-corrected for multiple comparisons.

subject threshold (minimum number of subjects for tagging a voxel as connected at the group level), and a curvature threshold (minimum allowed angle per streamline step, reflecting how "sharp" we allow streamline bends to be). In our main analysis above, we classified a striatal voxel as connected with a cortical site when at least 0.5/7 (human/macaque) out of 5,000 streamlines with a minimum curvature of 80° arrived at the cortical site in at least two out of nine subjects.

First, increasing the streamline threshold per individual subject two or three times did not alter our findings (Table 2). This suggests that differences between macaques and humans hold even when restricting our analyses to the corticostriatal fibers with the highest probability. Second, varying the subject threshold from one to all subjects did also not change our results (Fig. 4). This finding indicates that our conclusions hold even when focusing on corticostriatal fibers that are present in most or all subjects. Third, setting the fiber tracking minimum curvature threshold to 40 or 120° did not alter our main findings of more posterior connections in humans and more overlap for human FEF and M1 (Fig. 5). Nevertheless, overall less voxels are connected to cortical seeds when allowing sharp angles.

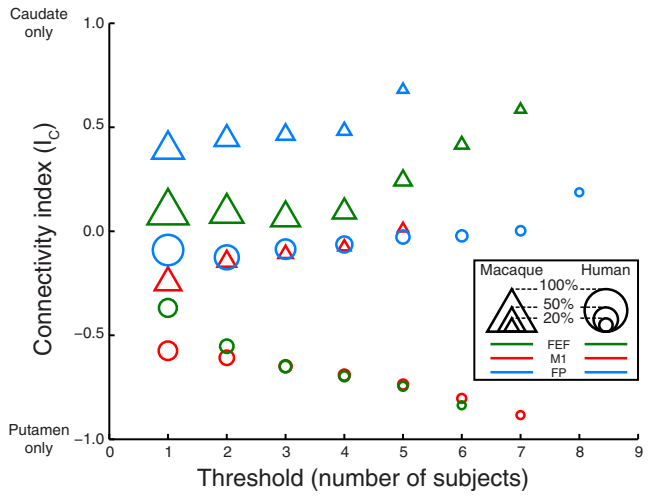

Fig. 4. Connectivity index connectivity index (I_C) as a function of group level probability threshold for data from M1 (red), FEF (green), and frontal pole (blue) from macaques (triangles) and humans (circles). This threshold reflects the number of subjects (humans or macaques) out of 7 for which a voxel was tagged at the single subject level that was needed to accept a voxel as being connected to the respective cortical seed at the group level. The size of each data point is proportional to the number of voxels on which the labeling index was computed. Data points for thresholds yielding connectivity <5% of the total striatal volume are not shown.

Taken together, these parameter variations along a large range of values indicate that the observed differences in connectivity between humans and macaques are likely to be genuine, as we cannot transform a macaque corticostriatal connectivity profile into a human profile by changing the most important fiber tracking parameters.

DISCUSSION

We report four new observations. First, in both macaques and humans the oculomotor and skeletomotor corticostriatal pathways terminate in both the caudate and putamen. Second, in humans the oculomotor pathway terminates in the putamen more than caudate. Third, in humans more than macaques the FEF and M1 termination zones in putamen overlap. Fourth, as a test of our approach we verified that frontal polar cortex connects with the anterior caudate. After interpreting these findings we consider potential problems and technical limitations.

Our comparative in vivo results are consistent both with recent results from studies of corticostriatal anatomical tract-tracing in macaques (Parthasaraty et al. 1992; Calzavara et al. 2008) and studies using DTI in humans (Neggers et al. 2012, Draganski et al. 2008; Verstynen et al. 2012). Together with Phillips and Everling (2012) who observed single unit saccade activation for macaques in the same anterior putamen region as we observed FEF connections, and putamen activation for saccades observed in human imaging studies (Dejardin et al. 1998; Krebs et al. 2010; Neggers et al. 2012), these findings confirm our hypothesis that primate FEF projects to both the caudate and putamen but with denser terminations in putamen for humans. The latter should be framed by the observation that the anatomical division of the striatum into the caudate and putamen is defined simply by the interruption of the striatum

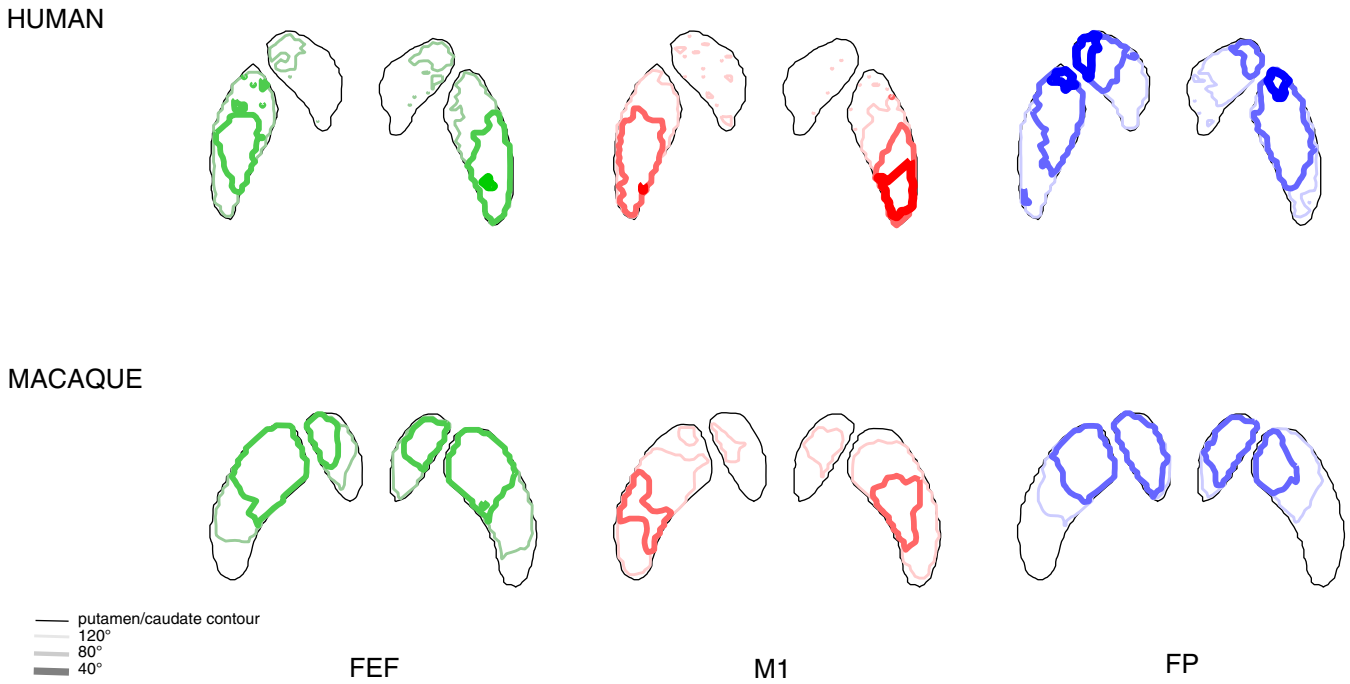

Fig. 5. The classification analysis was repeated for 3 different minimum curvature thresholds used during probabilistic tractography: 120° allowing only relatively straight streamlines, 80° (the default value used in all the other analyses in this study), and 40° allowing very sharp bends in assessed streamlines. *Top*: outlines of the putamen and caudate as thin black lines projected on an axial slice through the striatum for humans and in colored lines with increasing thickness (reflecting decreasing minimal curvature) the outlines of the zones connected to the cortical seeds from left to right for the FEF (in green), M1 (in red), and frontal pole (in blue). *Bottom*: same data for macaques.

by the internal capsule. Indeed, in rodents, there is no such anatomical distinction. Although striatal microcircuitry is reported to be relatively uniform (Gerfen et al. 1985), the macaque and human striatum can be divided into different neurochemical regions, which combine regions of the caudate and putamen into overlapping anatomo-functional territories (Parent and Hazrati 1995; Morel et al. 2002). The connectivity of FEF observed here in humans and macaques was to a common region characterized as the sensorimotor territory. Thus we surmise that any difference between species in gross corticostriatal anatomy need not indicate a difference of circuitry. In other words, we believe it likely that the neurons in human putamen receiving afferents from FEF project to substantia nigra and not globus pallidus, equivalent to projections from the macaque caudate nucleus (Hikosaka 2007).

In humans compared with macaques, projections from the FEF and M1 to the striatum appear to be shifted posteriorly. This is probably due to the enlargement of human prefrontal cortex through primate evolution (Semendeferi et al. 2001; Passingham and Wise 2012). The posterior shift of the FEF in the human brain compared with the macaque is evident in Figs. 2 and 3. Note that the pattern of FEF connectivity in humans is in agreement with findings obtained with a deterministic fiber tracking method applied to the same data (Neggers et al. 2012). As expected, we verified that the frontal pole in both humans and macaques connected with similar extents of the most anterior end of the striatum. This basic finding does not depend on the degree of homology of human and macaque polar cortex (e.g., Sallet et al. 2013; but see Bludau et al. 2013), but only demonstrates that the well-known A-P topography of corticostriatal connectivity was replicated.

Surprisingly, we also found greater overlap of oculomotor and skeletomotor regions in humans vs. macaques. This cannot be due to different relative voxel sizes with respect to brain size between species, as this would have predicted less overlap for humans. Perhaps an overlap of ocular and skeletal representations in putamen should not be surprising. Previous studies in macaques have described inputs to putamen from parietal visual areas (Cavada and Goldman-Rakic 1991) and neurons with both visual and tactile responses (Graziano and Gross 1993), information required for the control of eye, as well as hand movements. Whether this increased macroscopic overlap in humans suggests stronger functional integration of oculomotor and skeletomotor pathways at a microscopic level remains an open question. We speculate that this observed overlap may support greater eye-hand coordination that affords complex tool use, gesturing, and gaze following in humans; moreover, the consequences of human bipedal vs. macaque quadrapedal locomotion should be considered.

Several technical issues and limitations deserve consideration when interpreting these results. First, were the cortical seeds placed appropriately? We defined the monkey FEF as the anterior bank of the arcuate sulcus, which is a well-accepted definition (Bruce and Goldberg 1985; Stanton et al. 1989). For humans, we defined the FEF as the junction between the superior frontal sulcus and precentral sulcus. After initial debate, there now is ample support and consensus from neuroimaging work that in humans the functions generally attributed to the FEF are located at this junction (Amiez and Petrides 2009; Amiez et al. 2006; Neggers et al. 2012; Thakkar et al. 2014). The M1 seed was placed uncontroversially in the rostral bank of the central sulcus. Finally, the interpretation of the polar frontal seed does not depend on the degree of homology

of human and macaque polar cortex (e.g., Bludau et al. 2013; but see Sallet et al. 2013).

Second, we studied corticostriatal connectivity in the head and body of the caudate but not the tail. The tail is difficult to segment because of its small volume and convoluted shape, and the resolution of our DTI images was insufficient for reliably tracking fibers to this region.

Third, the acquisition protocols for macaques and humans were not entirely identical. Mainly, the monkeys were scanned at a lower effective resolution with respect to head size (despite much smaller absolute voxels for monkeys compared with humans), because the smaller voxels enclosed a larger fraction of brain volume. However, we equalized acquisition and analysis methods and adapted fiber reconstruction parameters as much as possible to make the results comparable. We further demonstrated the robustness of our main findings against tractography parameter changes.

In conclusion, compared with macaques, human oculomotor and skeletomotor corticostriatal fibers terminate more densely in the putamen than caudate, terminate in more posterior regions of the striatum, and overlapped to a much larger degree in humans. The interpretation of human imaging work in both the basic science and clinical domain typically assumes that corticostriatal circuitry is comparable between monkeys and humans. Our results indicate more caution is required when translating findings between nonhuman primates and humans. Whatever the functional consequences of the differences we found in corticostriatal connectivity, the differences are incompatible with well-known reviews (Alexander et al. 1986) and textbook descriptions (Purves et al. 2011; Kandel et al. 2012).

ACKNOWLEDGMENTS

We thank A. Maier for sharing imaging data, M. Feurtado and C. Suell for assistance with animal care, A. Anderson, D. Butler, and A. Newton for assistance with imaging and O. Hikosaka for helpful advice.

GRANTS

This work was supported by a grant from the Vanderbilt International Office; by National Institutes of Health Grants R01-EY-08890, R01-MH-55806, and P30-EY-08126; and by Robin and Richard Patton through the E. Bronson Ingram Chair of Neuroscience as well as a grant from the "Joint Programme" fund provided by Utrecht University (to S. F. W. Neggers).

DISCLOSURES

No conflicts of interest, financial or otherwise, are declared by the author(s).

AUTHOR CONTRIBUTIONS

Author contributions: S.F.W.N. and J.D.S. conception and design of research; S.F.W.N. and M.S.S. performed experiments; S.F.W.N., B.B.Z., M.S.S., and J.D.S. analyzed data; S.F.W.N., B.B.Z., and J.D.S. interpreted results of experiments; S.F.W.N. and B.B.Z. prepared figures; S.F.W.N. drafted manuscript; S.F.W.N., B.B.Z., M.S.S., and J.D.S. edited and revised manuscript; S.F.W.N., B.B.Z., M.S.S., and J.D.S. approved final version of manuscript.

REFERENCES

Alexander GE, DeLong MR, Strick PL. Parallel organization of functionally segregated circuits linking basal ganglia and cortex. *Annu Rev Neurosci* 9: 357–381, 1986.

Amiez C, Kostopoulos P, Champod AS, Petrides M. Local morphology predicts functional organization of the dorsal premotor region in the human brain. *J Neurosci* 26: 724–2731, 2006.

Amiez C, Petrides M. Anatomical organization of the eye fields in the human and non-human primate frontal cortex. *Prog Neurobiol* 89: 220–320, 2009.

Andersson JL, Skare S. A model-based method for retrospective correction of geometric distortions in diffusion-weighted EPI. *Neuroimage* 16: 177–199, 2002.

Ashburner J, Friston KJ. Unified segmentation. *Neuroimage* 26: 839–851, 2005.

Behrens TE, Berg HJ, Jbabdi S, Rushworth MF, Woolrich MW. Probabilistic diffusion tractography with multiple fibre orientations: what can we gain? *Neuroimage* 34: 144–155, 2007.

Behrens TE, Johansen-Berg H, Woolrich MW, Smith SM, Wheeler-Kingshott CA, Boulby PA, Barker GJ, Sillery EL, Sheehan K, Ciccarelli O, Thompson AJ, Brady JM, Matthews PM. Non-invasive mapping of connections between human thalamus and cortex using diffusion imaging. *Nat Neurosci* 6: 750–757, 2003.

Bludau S, Eickhoff SB, Mohlberg H, Caspers S, Laird AR, Fox PT, Schleicher A, Zilles K, Amunts K. Cytoarchitecture, probability maps and functions of the human frontal pole. *Neuroimage* 93: 260–275, 2014.

Bruce CJ, Goldberg ME. Primate frontal eye fields. I. Single neurons discharging before saccades. *J Neurophysiol* 53: 603–635, 1985.

Calzavara R, Mailly P, Haber SN. Relationship between the corticostriatal terminals from areas 9 and 46, and those from area 8A, dorsal and rostral premotor cortex and area 24c: an anatomical substrate for cognition to action. *Eur J Neurosci* 26: 2005–2024, 2007.

Cavada C, Goldman-Rakic PS. Topographic segregation of corticostriatal projections from posterior parietal subdivisions in the macaque monkey. *Neuroscience* 42: 683–696, 1991.

Connolly JD, Goodale MA, Cant JS, Munoz DP. Effector-specific fields for motor preparation in the human frontal cortex. *Neuroimage* 34: 1209–1219, 2007.

Dejardin S, Dubois S, Bodart JM, Schiltz C, Delinte A, Michel C, Roucoux A, Crommelinck M. PET study of human voluntary saccadic eye movements in darkness: effect of task repetition on the activation pattern. *Eur J Neurosci* 10: 2328–2336, 1998.

Draganski B, Kherif F, Klöppel S, Cook PA, Alexander DC, Parker GJ, Deichmann R, Ashburner J, Frackowiak RS. Evidence for segregated and integrative connectivity patterns in the human Basal Ganglia. *J Neurosci* 28: 7143–7152, 2008.

Dyrby TB, Søgaard LV, Parker GJ, Alexander DC, Lind NM, Baaré WF, Hay-Schmidt A, Eriksen N, Pakkenberg B, Paulson OB, Jelsing J. Validation of in vitro probabilistic tractography. *Neuroimage* 37: 1267–1277, 2007.

Fuster JM. *The Prefrontal Cortex*. London, UK: Academic, 2008.

Gerfen CR, Baimbridge KG, Miller JJ. The neostriatal mosaic: compartmental distribution of calcium-binding protein and parvalbumin in the basal ganglia of the rat and monkey. *Proc Natl Acad Sci USA* 82: 8780–8784, 1985.

Graziano MS, Gross CG. A bimodal map of space: somatosensory receptive fields in the macaque putamen with corresponding visual receptive fields. *Exp Brain Res* 97: 96–109, 1993.

Hikosaka O. Basal ganglia mechanisms of reward-oriented eye movement. *Ann NY Acad Sci* 1104: 229–249, 2007.

Kandel ER, Schwartz JH, Jessell TM, Siegelbaum SA, Hudspeth AJ. *Principles of Neural Science*. New York, NY: McGraw-Hill Professional, 2012.

Kennard C, Nachev P. Oculomotor dysfunction in Parkinson's disease. In: *Parkinson's Disease and Nonmotor Dysfunction*, edited Pfeiffer RD, Bodis-Wollner I. Totowa, NJ: Humana, 2005, p. 379–389.

Krebs RM, Woldorff MG, Tempelmann C, Bodammer N, Noesselt T, Boehler CN, Scheich H, Hopf JM, Duzel E, Heinze HJ, Schoenfeld MA. High-field fMRI reveals brain activation patterns underlying saccade execution in the human superior colliculus. *PLoS One* 5: e8691, 2010.

Markov NT, Ercsey-Ravasz M, Van Essen DC, Knoblauch K, Toroczkai Z, Kennedy H. Cortical high-density counterstream architectures. *Science* 342: 1238406, 2013.

McLaren DG, Kosmatka KJ, Oakes TR, Kroenke CD, Kohama SG, Matochik JA, Ingram DK, Johnson SC. A population-average MRI-based atlas collection of the rhesus macaque. *Neuroimage* 45: 52–59, 2009.

McLaren DG, Kosmatka KJ, Kastman EK, Bendlin BB, Johnson SC. Rhesus macaque brain morphometry: a methodological comparison of voxel-wise approaches. *Methods* 50: 157–165, 2010.

Morel A, Loup F, Magnin M, Jeanmonod D. Neurochemical organization of the human basal ganglia: anatomofunctional territories defined by the distributions of calcium-binding proteins and SMI-32. *J Comp Neurol* 443: 86–103, 2002.

Neggers SF, Van Diepen RM, Zandbelt BB, Vink M, Mandl RC, Gutteling TP. A functional and structural investigation of the human fronto-Basal volitional saccade network. *PLoS One* 7: e29517, 2012.

Parent A, Hazrati LN. Functional anatomy of the basal ganglia. I. The cortico-basal ganglia-thalamo-cortical loop. *Brain Res Rev* 20: 91–127, 1995.

Parthasarathy HB, Schall JD, Graybiel AM. Distributed but convergent ordering of corticostriatal projections: analysis of the frontal eye field and the supplementary eye field in the macaque monkey. *J Neurosci* 12: 4468–4488, 1992.

Passingham RE, Wise SP. *The Neurobiology of the Prefrontal Cortex: Anatomy, Evolution, and the Origin of Insight*. Oxford, UK: Oxford Univ. Press, 2012.

Paxinos G, Huang X, Toga, AW. *The Rhesus Monkey Brain in Stereotaxic Coordinates* (2000 ed.). San Diego, CA: Academic, 1999.

Phillips JM, Everling S. Neural activity in the macaque putamen associated with saccades and behavioral outcome. *PLoS One* 7: e51596, 2012.

Purves D, Augustine GJ, Fitzpatrick D, Hall WC, LaMantia AS, White LE. *Neuroscience* (5th ed.). New York: Sinauer, 2011.

Rex DE, Ma JQ, Toga AW. The LONI pipeline processing environment. *Neuroimage* 19: 1033–1048, 2003.

Rodriguez-Oroz MC, Jahanshahi M, Krack P, Litvan I, Macías R, Bezard E, Obeso JA. Initial clinical manifestations of Parkinson's disease: features and pathophysiological mechanisms. *Lancet Neurol* 8: 1128–1139, 2009.

Saleem KS, Logothetis NK. *A Combined MRI and Histology Atlas of the Rhesus Monkey Brain in Stereotaxic Coordinates* (2nd ed.). San Diego, CA: Elsevier/Academic, 2012.

Sallet J, Mars RB, Noonan MP, Neubert FX, Jbabdi S, O'Reilly JX, Filippini N, Thomas AG, Rushworth MF. The organization of dorsal frontal cortex in humans and macaques. *J Neurosci* 33: 12255–12274, 2013.

Semendeferi K, Armstrong E, Schleicher A, Zilles K, Van Hoesen GW. Prefrontal cortex in humans and apes: a comparative study of area 10. *Am J Phys Anthropol* 114: 224–241, 2001.

Smith SM, Jenkinson M, Woolrich MW, Beckmann CF, Behrens TE, Johansen-Berg H, Bannister PR, De Luca M, Drobnjak I, Flitney DE, Niazy RK, Saunders J, Vickers J, Zhang Y, De Stefano N, Brady JM, Matthews PM. Advances in functional and structural MR image analysis and implementation as FSL. *Neuroimage* 23, *Suppl* 1: S208–219, 2004.

Stanton GB, Deng SY, Goldberg ME, McMullen NT. Cytoarchitectural characteristic of the frontal eye fields in macaque monkeys. *J Comp Neurol* 282: 415–427, 1989.

Thakkar KN, van den Heiligenberg FM, Kahn RS, Neggers SF. Frontal-subcortical circuits involved in reactive control and monitoring of gaze. *J Neurosci* 34: 8918–8929, 2014.

Verstynen TD, Badre D, Jarbo K, Schneider W. Microstructural organizational patterns in the human corticostriatal system. *J Neurophysiol* 107: 2984–2995, 2012.

Yousry TA, Schmid ED, Alkadhi H, Schmidt D, Peraud A, Buettner A, Winkler P. Localization of the motor hand area to a knob on the precentral sulcus: a new landmark. *Brain* 120: 141–157, 1997.

Zilles K, Armstrong E, Schleicher A, Kretschmann HJ. The human pattern of gyrification in the cerebral cortex. *Anat Embryol (Berl)* 179: 173–179, 1988.

Zilles K, Armstrong E, Moser KH, Schleicher A, Stephan H. Gyrification in the cerebral cortex of primates. *Brain Behav Evol* 34: 143–150, 1989.